

# Examination of the InP/InGaAs Single-Photon Avalanche Diodes by Establishing a New TCAD-based Simulation Environment

Tihomir Knežević and Tomislav Suligoj

University of Zagreb, Faculty of Electrical Engineering and Computing, Croatia  
Micro and Nano Electronics Laboratory  
tihomir.knezevic@fer.hr

**Abstract**—Computational study of the InP/InGaAs single photon avalanche diode (SPAD) is performed using the additional numerical modeling employed as an extension to the TCAD software. A new simulation environment is employed to model the discrete events such as dark count rate (DCR) and photon detection efficiency (PDE) and is extensively tested for a range of temperatures and 1D structure parameters. DCR for SPAD with diffused Zn p<sup>+</sup> region operating at 200 K at 20 % PDE for 1.5 μm wavelength is 30 % lower compared to the DCR of structure with box-like p<sup>+</sup> region doping. The SPAD structures are also analyzed by transient simulations showing the impact of the external resistors on the response speed of the diodes.

**Keywords**—InP/InGaAs; SPAD; DCR; PDE; TCAD; simulation environment; process simulations; transient analysis

## I. INTRODUCTION

Single photon avalanche diodes (SPADs) employing the InP/InGaAs heterostructures are commonly used for low-light photon detection in the near-infrared range with wavelengths up to 1.7 μm. SPADs are operated in “Geiger” mode, biased above breakdown, and are capable of detecting a single photon that enters the device. Single photon counting for wavelengths above 1 μm is used, for example, in light detection and ranging (LIDAR) [1], quantum communication [2], optical time-domain reflectometry [3] and photon-correlation spectroscopy [4]. For proper SPAD operation, a quenching circuit [5] is needed to stop the avalanche and prepare the SPAD for the detection of a new photon.

In SPADs, self-sustained avalanche triggered by the photo-generated carriers is quantified by photon detection efficiency (PDE). Other than incoming photons, the avalanche can be triggered by unwanted processes such as thermally generated carriers, tunneling currents and background photons, which all increase a noise in the operation of the SPAD called dark count rate (DCR). The most common sources for DCR in a typically used separate absorption, grading, charge, multiplication (SAGCM) InP/InGaAs SPADs are thermally generated carriers from InP and InGaAs layers and trap-assisted tunneling (TAT) currents from InP region [6]. Parameters of the SAGCM structure, such as, doping concentrations and thicknesses of the regions could impact the magnitude of the TAT dark currents.

On the other hand, operating the SPAD at lower temperatures will decrease thermally generated DCR.

Modeling of the discrete characteristics of SPADs is not directly available from the simulation environment in commercially available TCAD simulators such as Sentaurus Device [7]. Analysis and simulations of the InP/InGaAs devices has been performed in the custom made simulators employing different analytical models for assessing the optical and electrical characteristics of SPADs [8]-[11]. None of the simulators offer the full functionality that could be achieved by using the TCAD software. Commercially available TCAD software has a large number of advanced physical models already included in the simulator together with various numerical methods for simulations of semiconductor devices. Process simulations of different fabrication steps could also be performed offering possibility for detailed analysis of SPADs with realistic doping profiles and various material composition.

In this work, additional numerical modeling, based on avalanche probability calculations, is employed as an extension to the functionality of the TCAD software. Physical models for InP, InGaAs and InGaAsP needed for SPAD simulations in TCAD are calibrated and validated in 200 K to 300 K temperature range. New TCAD-based environment is used for the examination of the characteristics of SPADs with InP and InGaAs materials.

## II. SPAD TCAD-BASED SIMULATION ENVIRONMENT

The goal of our analysis is to simulate the active part of the InP/InGaAs avalanche photodiode [12] in SPAD mode at low temperatures by combining the TCAD environment with our in-house numerical modeling to determine the DCR and PDE. Cross-section and doping profile of a commonly used avalanche photodiode operated in linear mode for near-infrared light detection is shown in Fig. 1.

### A. Calibration of the numerical computation procedure

In order to simulate the operation of APDs in Geiger mode, TCAD model for ionization coefficients in InP must be fitted. Impact ionization coefficients of the Okuto-Crowell model for InP are calibrated at different temperatures to the impact ionization coefficients from the quasi-physical analytical model which precisely fits the measurements [8]. Following

---

This work was supported by the Croatian Science Foundation under contract no. 9006.

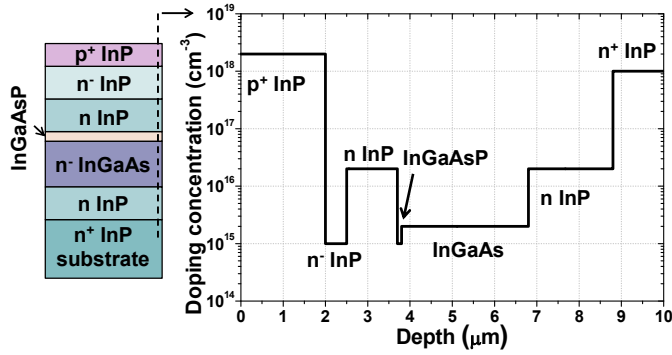


Fig. 1. Cross section and doping profile of the structure analyzed in the SPAD simulator.

Oldham et al. [13] we calculated the probabilities that a hole ( $P_h$ ) or an electron ( $P_e$ ) injected into the high-field region from any position in the structure ( $x$ ) will cause an avalanche:

$$\frac{dP_e}{dx} = (1 - P_e)\alpha_e(P_e + P_h - P_eP_h), \quad (1)$$

$$\frac{dP_h}{dx} = -(1 - P_h)\alpha_h(P_e + P_h - P_eP_h), \quad (2)$$

where  $\alpha_e$  and  $\alpha_h$  are impact ionization coefficients for electrons and holes, respectively. The  $\alpha_e$  and  $\alpha_h$  versus depth are extracted from TCAD simulator at different overbias voltages ( $V_{OB} = V_D - V_{BR}$ ). Impact ionization generation is turned off in the simulator and the bias voltages higher than breakdown voltage ( $V_{BR}$ ) can be simulated. Probability that a hole at the edge of the depletion region will generate an avalanche ( $P_H$ ) is simulated and shown in Fig. 2. Cross-section of the simulated structure is given in the inset and it corresponds to the structure from [8]. Calculated  $P_H$  for temperatures of 200, 240, 280 and 300 K are compared to the simulated data [8] and show excellent agreement.

DCR can be determined, using  $P_e$  and  $P_h$  combined with the carrier generation rate profiles ( $G_{dark}$ ) obtained from the TCAD simulator, by using the following equation:

$$DCR = \int_0^W P_{e(h)}(x) G_{dark}(x) dx, \quad (3)$$

where  $W$  is the depletion region width. The contributions of DCR mechanisms depend on particular SPAD structure [6], [9].

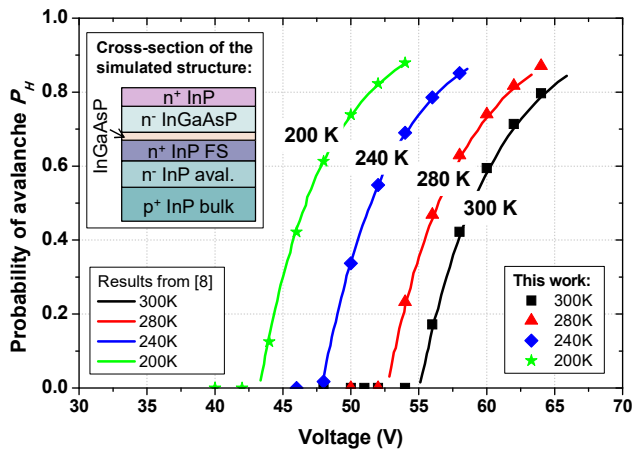


Fig. 2. Probability that a hole at the edge of the depletion region will initiate an avalanche compared to the results from [8]. Inset: simulated structure [8].

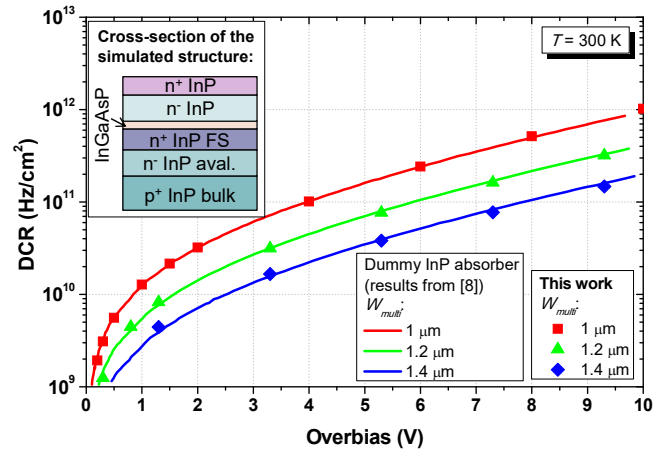


Fig. 3. Simulated DCR versus overbias voltage of the structure with dummy InP absorber compared to the results from [8]. Inset: simulated structure [8].

In this work, the included sources of DCR are SRH coming from all the materials in the stack, as well as TAT originating from InP. Parameters of the Schenk TAT model in TCAD have to be calibrated for InP such that it fits the measurements for different temperatures and device geometry parameters. The calculations of DCR versus overbias voltage are shown in Fig. 3 and compared to the measured results from [8]. The structures with a dummy InP absorber with different thicknesses of the multiplication region ( $W_{multi}$ ) are simulated and the parameters of TAT and SRH models in InP material are fitted to the data from [8]. The validity of the TAT generation model is also confirmed by the simulations of DCR for  $V_{OB} = 4$  V in the temperature range between 200 K and 300 K, as shown in Fig. 4. Calculated DCRs versus temperature, obtained by the fitted TAT model for InP, show excellent agreement to the measurements and simulation results from [8] for different thicknesses of the InP multiplication region. Parameters of the TCAD models for SRH from InGaAs and InGaAsP are also fitted and their contributions to DCR show excellent agreement for various temperatures and device geometry parameters as compared to the measured and simulated data in [9]-[12]. Fitting parameters of the TCAD models for TAT in InP and SRH in InP, InGaAs and InGaAsP are given in Table I.

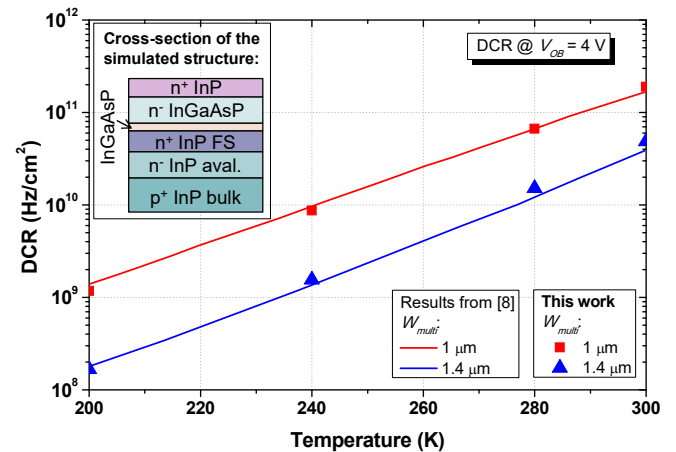


Fig. 4. Simulated DCRs at  $V_{OB} = 4$  V versus temperature compared to the results from [8]. Inset: simulated structure [8].

TABLE I. FITTING PARAMETERS FOR TCAD MODELS OF TAT IN INP AND SRH IN INP, INGAAS AND INGAASP

Model	Material	Parameters
SRH	InP	$E_T=0$ eV; $\tau_e=\tau_h=10^{-7}$ s
	InGaAs	$E_T=0.1$ eV; $\tau_e=\tau_h=4 \cdot 10^{-6}$ s
	InGaAsP	$E_T=0$ eV; $\tau_e=\tau_h=5 \cdot 10^{-6}$ s
TAT	InP	$E_T=0.34$ eV; $\tau_e=\tau_h=10^{-5}$ s; Schenk TAT parameters: $S=0.5$ ; $\hbar\omega=0.15$ eV; $m_{\theta,e}=m_{\theta,h}=0.043$

B. Analysis of the InP/InGaAs SPAD

Using the fitted model parameters for all the materials in the layer stack, we performed DCR simulations of the structure shown in Fig 1. at different temperatures. In Fig. 5, DCR contributions from InP, InGaAs and InGaAsP materials to the total DCR are plotted versus temperature at  $V_{OB} = 5$  V. Band-to-band tunnelling (BTBT) in InP and TAT in InGaAs are not included in the simulations. Dominant tunnelling mechanism in InP is TAT which is one or two orders of magnitude higher than BTBT [8]. The electric field magnitude in InGaAs is lower than the critical values to initiate TAT in this material [6]. DCR from InP starts to dominate the total DCR of the structure for the temperatures lower than 240 K. For higher temperatures, the DCR is determined as a sum of DCRs from InP and InGaAs. Very narrow multiplication region of only 0.5  $\mu\text{m}$  is dominating the TAT generation in InP.

Optical simulations of the structure are also performed and PDE is obtained using  $P_e$  and  $P_h$  together with the optical generation rate profiles ( $G_{photo}$ ):

$$OCR = \int_0^W P_{e(h)}(x) G_{photo}(x) dx, \quad (4)$$

$$PDE = \frac{OCR}{P}, \quad (5)$$

where  $P$  is the impinging photon flux. A complex refractive index of the  $\text{In}_{0.53}\text{Ga}_{0.47}\text{As}$  material [14] is also entered into the TCAD simulator. PDE versus wavelength is plotted in Fig. 6 for two different temperatures at  $V_{OB} = 5$  V. At lower wavelengths, PDE is higher at 200 K since the probabilities of starting an

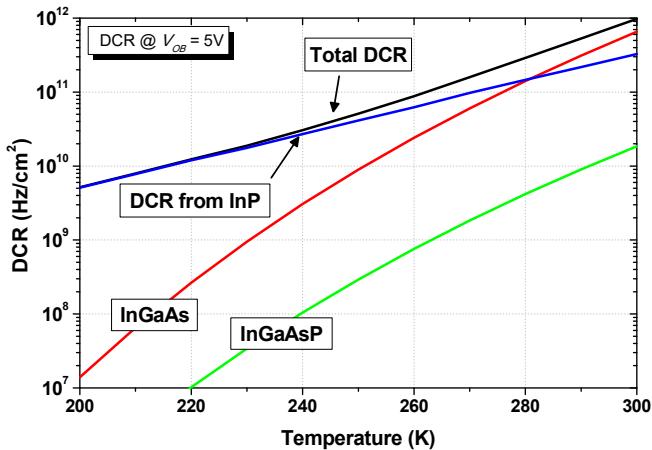


Fig. 5. Contribution to DCR from different materials in the layer stack at  $V_{OB} = 5$  V versus temperature.

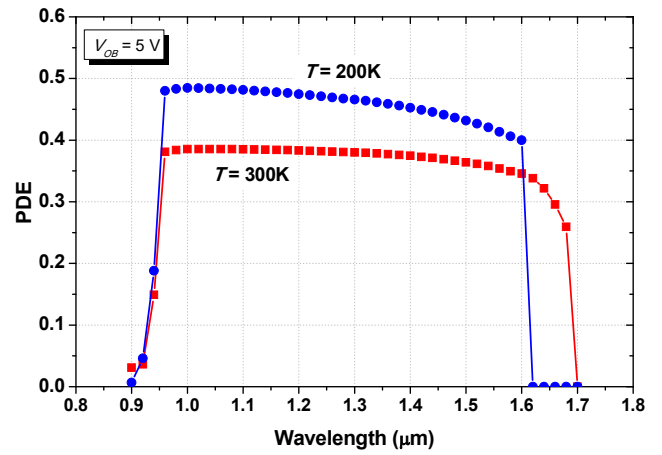


Fig. 6. PDE versus wavelength at  $V_{OB} = 5$  V for temperatures of 300 K and 200 K.

avalanche initiated by the optically generated carriers are higher at given  $V_{OB}$ . However, a total depletion region width in the absorbing region is smaller at 200 K so the PDE decrease is more pronounced with increasing wavelength, as compared to PDE at 300 K. DCR versus PDE is plotted in Fig. 7 for the device operating at 200 and 300 K and for the wavelengths of 1.5 and 1.1  $\mu\text{m}$ . The value of the DCR at PDE of 20 % for 1.1  $\mu\text{m}$  wavelength at 200 K is  $10^9$  Hz/cm<sup>2</sup>. The simulated structure is not optimized to work in a SPAD regime so rather high values of DCR are obtained even at low PDE and low temperature.

DCR versus PDE is also simulated for the structures with the  $p^+$  region with a realistic Zn-diffused profile. Simulation results are plotted in Fig. 8 for both structures operating at 200 K and 300 K for the wavelength of 1.5  $\mu\text{m}$ . Parameters for the process simulations of the Zn diffusion are obtained from [15]. The results show a larger difference in the DCR versus PDE between the two structures at 200 K. Zn-diffused profile used in the simulations results in a lower electric field compared to the structure with box-like  $p^+$  region. This will consequently decrease TAT. DCR at 20 % PDE for 1.5  $\mu\text{m}$  wavelength for the structure with diffused Zn profile decreases by 30 % at 200 K compared to the DCR of the structure with box-like  $p^+$  region.

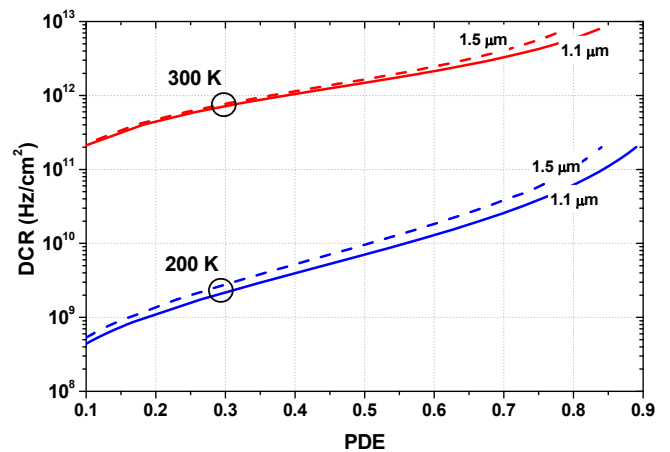


Fig. 7. DCR vs. PDE for wavelengths of 1.5 and 1.1  $\mu\text{m}$  and for temperatures of 200 K and 300 K.

## III. CONCLUSIONS

Computational study of the InP/InGaAs SPAD diode is performed using the functionality of the TCAD software which is extended to model the discrete events such as DCR and PDE. This novel simulation method is extensively tested for a range of temperatures and 1D structure parameters and shows excellent agreement to the measurements. Process simulations of Zn diffusion are also performed to obtain realistic  $p^+$  region doping profiles resulting in a decreased DCR comparing to the diode with box-like  $p^+$  region. Process simulations of Zn diffusion together with discrete SPAD characteristics make the simulator environment capable for the 2D simulations of realistic SPAD devices. New TCAD environment can also be used for transient simulations of SPADs making it possible to add an external resistor for passive quenching circuit and analyze its impact on the response speed.

## REFERENCES

- [1] U. Schreiber, C. Werner, "Laser Radar Ranging and Atmospheric Lidar Techniques", Proceedings of SPIE, SPIE, 1997, Dec. 1997
- [2] N. Gisin and R. Thew, "Quantum communication," Nature Photon., vol. 1, no. 3, pp. 165–171, Mar. 2007.
- [3] P. Eraerds, M. Legre, J. Zhang, H. Zbinden, and N. Gisin, "Photon counting OTDR: Advantages and limitations," J. Light. Technol., vol. 28, no. 6, pp. 952–964, Mar. 2010.
- [4] R. G. W. Brown, K. D. Ridley, and J. G. Rarity, "Characterization of silicon avalanche photodiodes for photon-correlation measurements. I: Passive quenching," Appl. Opt., vol. 25, no. 22, pp. 4122–4126, Nov. 1986.
- [5] S. Cova, M. Ghioni, A. Lacaita, C. Samori, and F. Zappa, "Avalanche photodiodes and quenching circuits for single-photon detection," Applied Optics, Vol. 35, Issue 12, pp. 1956–1976, 1996.
- [6] F. Acerbi, M. Anti, A. Tosi and F. Zappa, "Design Criteria for InGaAs/InP Single-Photon Avalanche Diode" IEEE Photonics Journal, vol. 5, no. 2, pp. 6800209–6800209, April 2013.
- [7] Sentaurus Device User Guide, Synopsys, Mountain View, CA, USA, Mar. 2016.
- [8] J. P. Donnelly et al., "Design Considerations for 1.06- $\mu\text{m}$  InGaAsP-InP Geiger-Mode Avalanche Photodiodes" IEEE Journal of Quantum Electronics, vol. 42, no. 8, pp. 797–809, Aug. 2006.
- [9] X. Jiang, M. A. Itzler, R. Ben-Michael and K. Slomkowski, "InGaAsP-InP Avalanche Photodiodes for Single Photon Detection", IEEE Journal of Selected Topics in Quantum Electronics, vol. 13, no. 4, pp. 895–905, July–aug. 2007.
- [10] M. Anti, F. Acerbi, A. Tosi and F. Zappa, "2D simulation for the impact of edge effects on the performance of planar InGaAs/InP SPADs", Proc. SPIE 8550, Optical Systems Design 2012, pp. 855025–855025-10
- [11] M. Anti, F. Acerbi, A. Tosi and F. Zappa, "Integrated simulator for single photon avalanche diodes," Numerical Simulation of Optoelectronic Devices (NUSOD), 2011 11th International Conference on, Rome, 2011, pp. 47–48
- [12] Y. Liu et al., "A planar InP/InGaAs avalanche photodiode with floating guard ring and double diffused junction" Journal of Lightwave Technology, vol. 10, no. 2, pp. 182–193, Feb 1992.
- [13] W. G. Oldham, R. R. Samuelson and P. Antognetti, "Triggering phenomena in avalanche diodes, IEEE Trans. Electron Devices vol. ED-19, pp. 1056–1060, Sept. 1972.
- [14] S. Adachi, "Physical Properties of III-V Semiconductor Compounds: InP, InAs, GaAs, GaP, InGaAs, and InGaAsP", John Wiley & Sons, 1992
- [15] T. Knežević, T. Suligoj, "Analysis of Electrical and Optical Characteristics of InP/InGaAs Avalanche Photodiodes in Linear Regime by a New Simulation Environment", Proc. of the 39th International Convention MIPRO 2016, pp. 34–39, Rijeka, Croatia

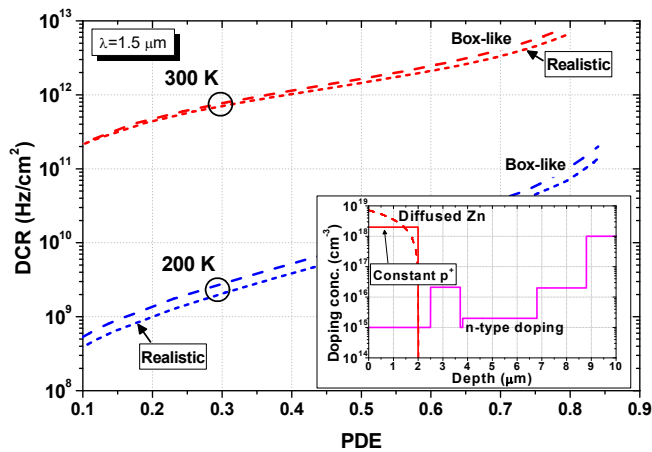


Fig. 8. DCR vs. PDE for the structures with box-like and realistic Zn-diffused profiles. Inset: Comparison of the box-like and realistic Zn-diffused profiles.

Transient simulations of SPADs with InP and InGaAs are performed using the established TCAD environment. Transient simulations provide additional information on the design of the quenching circuits and optimization of the structure to achieve a faster response of SPAD. Diode is biased at  $V_{OB} = 5$  V and the optical pulse is generated at  $t = 10^{-12}$  s. SRH is turned off to prevent triggering of the avalanche. Transient response of the photocurrent is plotted in Fig. 9 for different values of the resistor in series to the analyzed diode (basic passive quenching circuit). The increase of the diode current is caused by the avalanche process when the optically generated carriers enter the multiplication region. Probabilities of triggering an avalanche are not used in these simulations. The values of the resistors of 1 k $\Omega$  and 100 k $\Omega$  are not sufficient to quench the diode, and the diode is in the quasi-stationary state where the avalanche could not be stopped. This is also confirmed by transient response of diode overbias voltage for the same values of the external resistors plotted in the inset in Fig. 9. External resistor with 100 k $\Omega$  can decrease the diode voltage below  $V_{OB} = 0$  V for a short period of time, which is, however, not long enough to remove all the charge generated in the avalanche process. Return of the diode voltage above the breakdown causes the avalanche process to continue preventing the quenching of the diode.

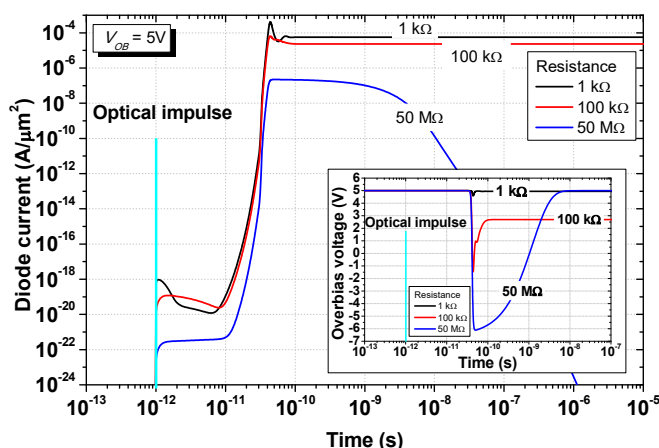


Fig. 9. Transient response of the diode current for values of the passive quenching circuit resistance of 1 k $\Omega$ , 100 k $\Omega$  and 50 M $\Omega$ . Inset: transient response of the diode overbias voltage.